The Astrophysical Journal, 628:L127–L130, 2005 August 1
© 2005. The American Astronomical Society. All rights reserved. Printed in U.S.A.

CHANDRA OBSERVATIONS OF SHOCK KINEMATICS IN SUPERNOVA REMNANT 1987A

S. A. Zhekov,[1,2] R. McCray,[1] K. J. Borkowski,[3] D. N. Burrows,[4] and S. Park[4]

Received 2005 May 16; accepted 2005 June 17; published 2005 July 13

ABSTRACT

We report the first results from deep X-ray observations of the supernova remnant SNR 1987A with the *Chandra* LETG. Temperatures inferred from line ratios range from ~0.1 to 2 keV and increase with ionization potential. Expansion velocities inferred from X-ray line profiles range from ~300 to 1700 km s^{-1}, much less than the velocities inferred from the radial expansion of the radio and X-ray images. We can account for these observations with a scenario in which the X-rays are emitted by shocks produced where the supernova blast wave strikes dense protrusions of the inner circumstellar ring, which are also responsible for the optical hot spots.

Subject headings: supernova remnants — supernovae: general — supernovae: individual (SNR 1987A) — X-rays: ISM

1. INTRODUCTION

With the rapidly developing impact of the debris of supernova SN 1987A with its inner circumstellar ring, we have an unprecedented opportunity to witness the birth of a supernova remnant, SNR 1987A (McCray 2005). This event, the first hint of which was the 1995 appearance of spot 1, a rapidly brightening optical "hot spot" on the ring, has now evolved into the stage where the ring is encircled by hot spots (Sugerman et al. 2002). Additionally, an annular source of X-ray emission correlated with the locations of the hot spots has brightened at an accelerating rate (Park et al. 2004). Evidently, the optical hot spots appear where the supernova blast wave encounters fingers of relatively dense gas protruding inward from the ring. In such a situation, a complex hydrodynamic interaction ensues (cf. Borkowski et al. 1997a, 1997b). The optical emission from the spots comes from relatively slow ($V_S \leq 200$ km s^{-1}) shocks that have had time to undergo radiative cooling (Pun et al. 2002). The X-ray emission must come from gas heated by faster ($V_S \geq 1000$ km s^{-1}) shocks, either transmitted shocks entering the protrusions or shocks reflected from the protrusions.

Michael et al. (2002) reported the first observation of a dispersed X-ray spectrum of SNR 1987A, taken in October 1999 with HETG on *Chandra*. The X-ray emission was dominated by shock-heated gas having an electron temperature $kT_e \approx 2.6$ keV. Due to the poor photon statistics, only a composite line profile was constructed by stacking the profiles of the individual observed lines. From the measured FWHM (≈5000 km s^{-1}), they inferred that the X-ray–emitting gas was moving with a radial velocity of ≈3500 km s^{-1}, roughly the same as that inferred from the observed proper motion of the nonthermal radio source (Manchester et al. 2002) and the X-ray source (Park et al. 2004).

From 1999 October to 2004 September, the X-ray source SNR 1987A has brightened by a factor of ~10 (Park et al. 2005). As a result, it has become possible with *Chandra* to obtain dispersed X-ray spectra with very high counting statistics. In this Letter, we report the first results from the analysis of such observations.

[1] JILA, University of Colorado, UCB 440, Boulder, CO 80309-0440; zhekovs@colorado.edu, dick@jila.colorado.edu.

[2] On leave from the Space Research Institute, Sofia, Bulgaria.

[3] Department of Physics, North Carolina State University, P.O. Box 8202, Raleigh, NC 27695-8202; kborkow@unity.ncsu.edu.

[4] Department of Astronomy and Astrophysics, Pennsylvania State University, 525 Davey Laboratory, University Park, PA 16802; burrows@astro.psu.edu, park@astro.psu.edu.

2. OBSERVATIONS AND DATA REDUCTION

SNR 1987A was observed with *Chandra* in the LETG ACIS-S configuration in five consecutive runs during 2004 August 26–September 5, providing a total effective exposure of 289 ks. We extracted[5] positive and negative first-order LETG spectra for each of the five observations. Then we merged the resultant spectra into one spectrum each for the positive and negative LETG arms with respective total counts of 9241 and 6057 in the energy range 0.4–7 keV. The difference in photon statistics is a result of the different sensitivities of the respective CCD detectors. We also extracted the pulse-height spectrum from the zeroth-order image with a total number of 16,557 counts in the 0.4–7 keV range. Figure 1 demonstrates the enormous scientific advantage of the dispersed spectrum over the pulse-height spectrum.

We fitted the strong emission line triplets of various He-like ions by a sum of three Gaussians and a constant local continuum. The ratio of line centers of the triplet components is held fixed according to the values given by the *Chandra* atomic database (see footnote 5), and all components shared the same FWHM. Thus, the free parameters were the intensities of their components, the line-center wavelength of one of the components, FWHM, and the local continuum. Likewise, we fitted the strong emission doublets of the H-like species, but the component intensities were fixed through their atomic data values. We found that the centroid shifts for the strong emission lines were consistent with the redshift of the LMC and that the line fluxes derived from the positive and negative first-order spectra agreed within expected statistical uncertainties. Therefore, we assumed that all the line centers had the same Doppler shift, $V_D = 286$ km s^{-1}, and fitted the positive and negative first-order spectra simultaneously.

3. LINE FLUXES AND RATIOS

Table 1 lists the fluxes of all the emission lines and multiplets that could be measured with acceptable photon statistics. Given the excellent spectral resolution and photon statistics, we can for the first time derive reliable intensities and ratios of various X-ray emission lines from SNR 1987A. As we shall discuss in § 5, we expect the actual conditions in the plasma to be sufficiently complex that we can only use the line strengths and ratios to infer the typical conditions of the plasma re-

[5] For CIAO 3.1 and ATOMDB, see http://cxc.harvard.edu/ciao and http://cxc.harvard.edu/atomdb.

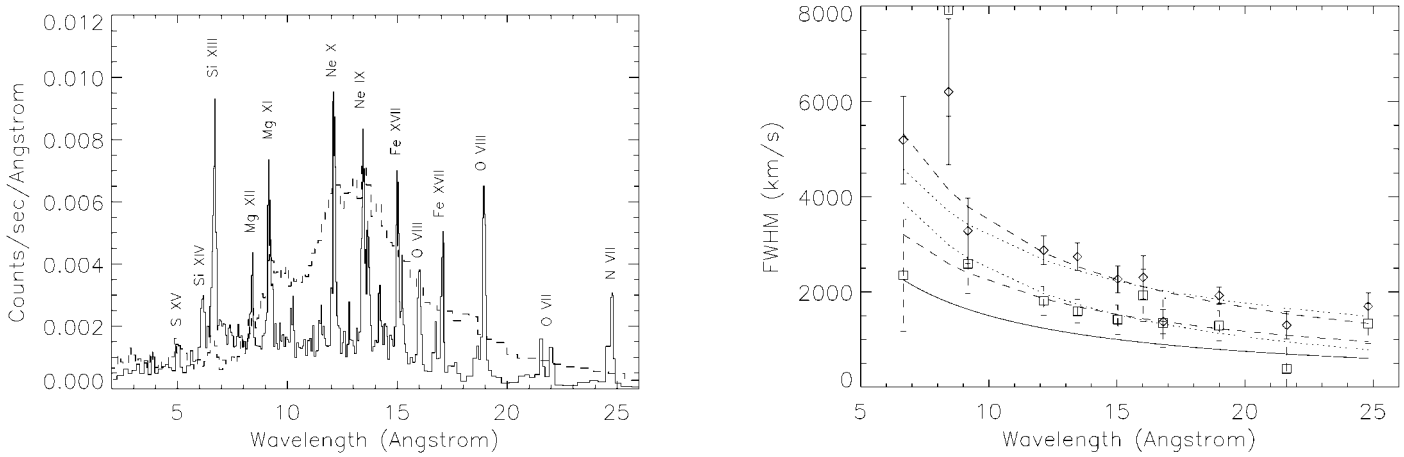


FIG. 1.—*Left panel*: Background-subtracted LETG first (+1, *solid line*) and zeroth-order (*dashed line*) spectra. *Right panel*: Measured line widths (FWHM) for the positive (*diamonds*) and negative (*squares*) LETG arms. The solid curve represents the resolving power of the LETG ($E/\Delta E \approx 20\lambda$). The dashed and dotted curves correspond to the line-broadening parameter in the cases with and without shock stratification (see § 4).

sponsible for the emission by a given ion. The ratio of He-like (Kα) to H-like ions (Lyα) from a given element is sensitive to both the temperature and the ionization state of the gas. The same is true for the "*G*-ratio" of the He-like triplet lines [$G = (f + i)/r$, where *f*, *i*, and *r* stand for forbidden, intercombination, and recombination lines, respectively] since these lines are produced not only by electron impact excitation of the He-like ions but also by K-shell ionization of the Li-like ions (Mewe 1999; Liedahl 1999).

Since we expect that shocks are responsible for heating and ionizing the X-ray–emitting gas, we can compare our measured line ratios to those resulting from the XSPEC code, which provides models of the time-dependent ionization and X-ray emission from plane-parallel shocks (Borkowski et al. 2001). In such models, the line ratios are functions of the postshock temperature and the ionization age, $n_e t$, defined as the time since the gas first entered the shock times the postshock electron density. The X-ray–emitting plasma in SNR 1987A is in nonequilibrium ionization, and so inner-shell ionization and excitation contribute importantly to emission-line ratios. Indeed, if these processes are not included, the theoretical *G*-ratios cannot match the observed ones.

In Figure 2, the curves define those regions in the parameter space of electron temperature and ionization age, $n_e t$, for which the observed line ratios agree with the ratios that would result from a plane-parallel shock. Except for a very narrow range of $n_e t$, the inferred temperatures are likely to be in the range 0.1–2 keV. We see immediately that no single combination of electron temperature and ionization age is consistent with all the observed ratios. Instead, for any given ionization age, the inferred electron temperature increases tentatively with ionization potential. Evidently, the X-ray emission comes from a distribution of shocks having a range of ionization ages and postshock temperatures.

4. LINE PROFILES

The excellent spatial and spectral resolution of *Chandra* allows us for the first time to observe the kinematics of the X-ray–emitting gas through the line profiles. The method is illustrated in Figure 3.[6] We assume that the X-ray source lies on a circular ring having an angular radius θ_R and that this ring is expanding with constant radial velocity, V_R. We also assume that the X-ray source has, like the optical inner circumstellar

[6] For the general properties of LETG, see § 9 of the *Chandra* Proposer's Observatory Guide, ver. 7.0, p. 195; the complexity of the spatial-spectral effects is discussed in § 8.5.3, pp. 187–189 and § 9.3.3, pp. 209–215.

TABLE 1
SNR 1987A: LINE FLUXES

Line	Ionization Potential (keV)	λ_{lab}[a] (Å)	Flux[b] (10^{-6} photons cm^{-2} s^{-1})	Counts[c]
S XV Kα	3.22	5.0387	5.14 ± 2.15	87.5 ± 36.6
Si XIV Lyα	2.67	6.1804	2.22 ± 0.46	102.7 ± 21.3
Si XIII Kα	2.44	6.6479	11.86 ± 1.19	522.7 ± 52.4
Mg XII Lyα	1.96	8.4192	7.33 ± 0.96	250.6 ± 32.8
Mg XI Kα	1.76	9.1687	18.09 ± 1.11	475.7 ± 29.2
Ne X Lyα	1.36	12.1321	36.40 ± 2.40	552.3 ± 36.4
Ne IX Kα	1.20	13.4473	60.68 ± 3.82	838.2 ± 52.8
Fe XVII[d]	1.27	15.0140	38.10 ± 3.20	450.4 ± 37.7
O VIII Lyβ	0.87	16.0055	19.90 ± 2.40	204.7 ± 24.7
Fe XVII[d]	1.27	16.7800	24.14 ± 3.18	336.4 ± 37.8
O VIII Lyα	0.87	18.9671	50.80 ± 4.00	377.3 ± 29.7
O VII Kα	0.74	21.6015	35.20 ± 5.77	162.8 ± 26.7
N VII Lyα	0.67	24.7792	44.90 ± 5.20	203.7 ± 23.6

[a] The laboratory wavelength of the main component.
[b] The observed total line/multiplet flux and the associated 1 σ errors.
[c] The total number of counts in all components of a spectral line (continuum-subtracted).
[d] The total flux from the strongest component $\lambda\lambda$15.01, 15.26 and $\lambda\lambda$16.78, 17.05, 17.10, respectively.

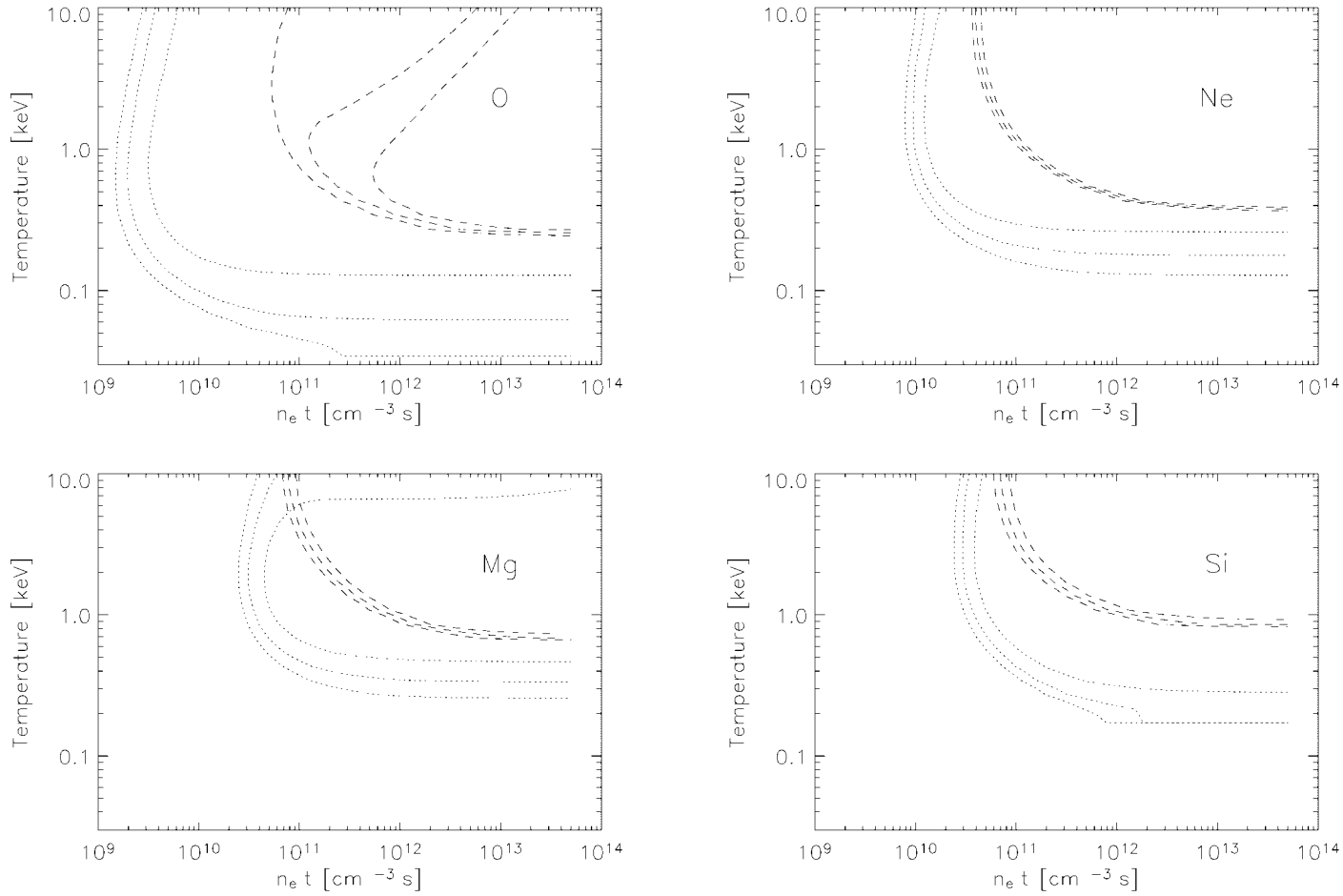


FIG. 2.—Isolines of the *G*-ratios (*dotted curves*) and the Kα/Lyα ratios (*dashed curves*) for O, Ne, Mg, and Si. Note that the *G*-ratios include the line contribution from inner-shell processes (see text). The three curves for each ratio correspond to the measured value and $\pm 1\ \sigma$. The Kα/Lyα ratios have been corrected for differential X-ray absorption assuming $N_{\rm H} = 1.6 \times 10^{21}$ cm^{-2}. The observed *G*-ratios are 1.44 ± 0.47 (O), 0.87 ± 0.11 (Ne), 0.79 ± 0.09 (Mg), and 1.17 ± 0.23 (Si).

ring, an inclination angle $i = 44°$–$45°$, with the near side to the north and a minor axis at P.A. $\approx 354°$ (Sugerman et al. 2002). The roll angle was chosen so that the negative ($m = -1$) arm of the dispersion axis was aligned at P.A. $\approx 345°$; thus, the north side of the ring will be blueshifted, and the south side will be redshifted. The dispersed images of the ring will be distorted by these Doppler shifts (see footnote 6). In the $m = -1$ image, the northern side of the ring will be displaced to the left, and the southern side will be displaced toward the right. Thus, the minor axis of the $m = -1$ image will be compressed. Likewise, the minor axis of the $m = +1$ image will be stretched.

This behavior is exactly what we see in the measured line profiles. We fitted Gaussian profiles (as explained in § 2) to each emission line or multiplet independently in the $m = +1$ and $m = -1$ first-order spectra. In every case, the width of a given emission line in the $m = +1$ arm is greater than the corresponding width in the $m = -1$ arm (Fig. 1). The actual line profile will likely differ from a Gaussian due to the complex spatial-spectral effects. However, the Gaussian approximation is sufficient for the analysis presented here (resulting in a reduced $\chi^2 \approx 1$ for each of the line-profile fits).

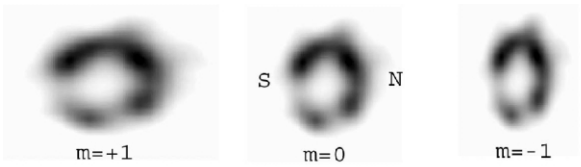


FIG. 3.—Schematic view of the LETG observational situation for SNR 1987A using the deconvolved zeroth-order total image. The X-ray source is assumed to be an inclined ring, the northern (N) side of which is blueshifted and the southern (S) side of which is redshifted. Shown are the zeroth-order image ($m = 0$) as well as the positive ($m = +1$) and negative ($m = -1$) images in an arbitrary spectral line. The dispersion direction is horizontal.

There are two major sources of line broadening in the dispersed images. One is the spatial extent of the image itself, which can be expressed as an equivalent line broadening, independent of wavelength. The second is the broadening due to the bulk motion of the shocked gas. We express the net line width (FWHM) broadening as

$$\Delta\lambda_{\rm tot} = 2\Delta\lambda_0 \pm 2z_0(\lambda/\lambda_0)^{\alpha}\lambda, \qquad (1)$$

where the plus (minus) sign refers to the $m = +1$ ($m = -1$) spectrum. The two sources of broadening are represented, respectively, by the first and second terms on the right-hand side of equation (1). The power-law function of wavelength allows for the possibility that the mean bulk velocity of shocked gas emitting a given line may depend on the excitation or ionization stage of the emitting ion. The parameter z_0 determines the line broadening at some fiducial wavelength, λ_0, and the power-law index α is to be determined.

We then fit equation (1) to the data in Figure 1. We consider

two models. In the first (constant velocity) model, we assume that all emitting ions have the same mean bulk velocity ($\alpha = 0$). In that case, we find a best-fit value $z_0 = 0.0006$. In the second (stratified) model, we allow the values of α and z_0 to vary. In that case, we find a best-fit value $\alpha = -1.3$. Note that such a negative value of α implies that emission lines with shorter wavelength are produced by gas having greater radial velocity, as expected. The stratified model provides a slightly better fit to the data than the constant velocity model (χ^2/dof = 22/19 vs. 25/20), but the data are not good enough to distinguish between the models with confidence. We may translate the fitting parameters into an equivalent mean radial bulk velocity, V_r, of an expanding circular ring by adopting an average value for the azimuthal ϕ ($\overline{\sin\phi} = 2/\pi$, $0 \le \phi \le \pi/2$) and a value ($i = 45°$) for the inclination of the inner ring. This yields a value $V_r = 397$ km s^{-1}. In the case of a strong radial shock with adiabatic index $\gamma = 5/3$, the corresponding shock velocity must be $V_S = 4V_r/3 = 530$ km s^{-1} . The corresponding shock velocity in the stratified case is given by $V_S(\lambda) = 920(\lambda/10\ \text{Å})^{-1.3}$ km s^{-1}. Finally, we note that in the both models, the derived source half-size of $\Delta\lambda_0 = 0.047$ Å or $\theta_R = 0\farcs84$ is consistent with the SNR 1987A size from an X-ray image-deconvolution technique (Burrows et al. 2000). Thus, we are confident that the simplified treatment presented here gives reliable results.

5. DISCUSSION AND CONCLUSIONS

The most surprising result of this observation is the relatively low velocity of the X-ray–emitting gas as determined from the line profiles. When we proposed to do this observation, we expected to see kinematic velocities in the range ~2500–3000 km s^{-1}, as we saw in the composite line profile measured with the *Chandra* HETG in 1999 October (Michael et al. 2002) and in the radial expansion rate of the X-ray image (Park et al 2004). At the very least, we would expect to see velocities comparable to the velocity of gas behind a shock moving sufficiently fast to heat the electrons to temperatures inferred from the X-ray line ratios. For a shock of high Mach number entering stationary gas with velocity V_S, the maximum electron temperature is $kT_e = (3/16)\mu V_S^2 = 1.4(V_S/1000\ \text{km s}^{-1})^2$ keV. The value $V_S = 530$ km s^{-1} inferred for the constant velocity model then implies a postshock temperature $kT_e \le 0.39$ keV. This value is inconsistent with the temperatures required to account for the Kα/Lyα line ratios observed for Mg and Si (Fig. 2). On the other hand, the electron temperatures inferred from the line profiles in the stratified model may be consistent with the observed line ratios ($kT_e = 0.15$–4.0 keV for $V_S = 340$–1700 km s^{-1}).

How do we reconcile the relatively low gas velocities inferred from the line profiles with the much greater velocities inferred from the radial expansion rate of the X-ray image? We have in mind a picture in which a blast wave of velocity $V_B \sim 3000$ km s^{-1} propagates through the low atomic density ($n_0 \sim 100$ cm^{-3}) gas inside the circumstellar ring. A zone of enhanced X-ray emission appears when the blast wave strikes a finger of relatively dense ($n_1 \sim 3 \times 10^3$–3×10^4 cm^{-3}) gas protruding inward from the ring. A transmitted shock propagates into the protrusion at a velocity reduced by a factor $\sim(n_1/n_0)^{1/2}$, while a reflected shock propagates backward. The latter increases the density and temperature of the circumstellar matter to values substantially greater than those caused by the original blast wave, and it also reduces the radial velocity of the doubly shocked circumstellar gas. The enhanced X-ray emission comes from the gas behind the transmitted shock and from the gas behind the reflected shock, with the proportional contributions depending on the details of the hydrodynamics. But the lower velocity of the transmitted shock and the high density behind it ensure a short cooling timescale and eventually increased optical emission. At each point of impact with a protrusion, a new zone of enhanced X-ray emission appears. Thus, the mean radius of the enhanced X-ray emission appears to move outward at a substantial fraction of the blast wave velocity, while the gas responsible for most of the X-ray emission may be moving much more slowly. This picture assumes that only a small fraction of the blast wave area is covered by protrusions at the present time. It also implies that the radial expansion of the X-ray image should slow down rapidly as the blast wave overtakes the entire equatorial ring.

The scenario that we have described here accounts in a natural way for several properties observed by *Chandra* images and spectra of SNR 1987A: (1) the correlation of the rapid X-ray brightening with the appearance of the optical hot spots; (2) the correlation of the X-ray image with the optical hot spots; (3) the relatively rapid expansion of the X-ray image compared to the relatively slow bulk velocity of the X-ray–emitting gas; and (4) the correlation of the inferred electron temperature and expansion velocity of the shocked gas with the excitation potential of X-ray emission lines.

There is much more to be learned from the *Chandra* spectroscopic data beyond the brief summary that we have presented here. By fitting global models for the entire X-ray spectrum, we can infer element abundances and the distribution of the emission measure with temperature. By simulating the actual two-dimensional images in the dispersed spectra (e.g., with the MARX software), we can refine our models of the kinematics and spatial distribution of the shocked gas. By constructing simulations of the hydrodynamics of the impact of the blast wave with the protrusions, we hope to provide a more refined interpretation of the observations than the analysis presented here.

This work was supported by NASA through *Chandra* Awards G04-5072A (to CU, Boulder, CO) and GO4-5072B (to NCSU, Raleigh, NC). The authors appreciate the careful reading and comments by an anonymous referee.

REFERENCES

Borkowski, K. J., Blondin, J. M., & McCray, R. 1997a, ApJ, 476, L31
———. 1997b, ApJ, 477, 281
Borkowski, K. J., Lyerly, W. J., & Reynolds, S. P. 2001, ApJ, 548, 820
Burrows, D. N., et al. 2000, ApJ, 543, L149
Liedahl, D. A. 1999, in X-Ray Spectroscopy in Astrophysics, ed. J. van Paradijs & J. A. M. Bleeker (Lecture Notes in Phys. 520; New York: Springer), 189
Manchester, R. N., Gaensler, B. M., Wheaton, V. C., Staveley-Smith, L., Tzioumis, A. K., Bizunok, N. S., Kesteven, M. J., & Reynolds, J. E. 2002, Publ. Astron. Soc. Australia, 19, 207
McCray, R. 2005, in IAU Colloq. 192, Cosmic Explosions, ed. J. M. Marcaide & K. W. Weiler (Heidelberg: Springer), 77
Mewe, R. 1999, in X-Ray Spectroscopy in Astrophysics, ed. J. van Paradijs & J. A. M. Bleeker (Lecture Notes in Phys. 520; New York: Springer), 109
Michael, E., et al. 2002, ApJ, 574, 166
Park, S., Zhekov, S. A., Burrows, D. N., Garmire, G. P., & McCray, R. 2004, ApJ, 610, 275
———. 2005, Adv. Space Res., in press (astro-ph/0501561)
Pun, C. S. J., et al. 2002, ApJ, 572, 906
Sugerman, B. E. K., Lawrence, S. S., Crotts, A. P. S., Bouchet, P., & Heathcote, S. R. 2002, ApJ, 572, 209